Modelling of Delamination and Debonding in Laminated Composites using a Moving Mesh Approach

S. J. Lord[1] & E. S. Greenhalgh[2]

[1]*Future Systems Technology, QinetiQ, Farnborough, Hampshire, UK, GU14 0LX.*
[2]*The Composites Centre, Imperial College London, UK, SW7 2AZ*

Abstract

Laminated materials are used in a wide range of applications, but their uptake for primary (safety-critical) components has been limited partly by a shortage of reliable and robust models for predicting the performance of delaminated structures. Modelling of delamination and debonding is computationally demanding, with issues such as large deformations, local buckling of the delaminated layers, global buckling of the entire structure and contact across the crack faces needing to be addressed. The conventional approach to delamination growth is to use node release; but this approach can be problematic. This paper describes an alternative approach to delamination modelling; the moving mesh in which the crack front is advanced automatically by moving nodes. This approach is demonstrated against two experimental benchmarks representative of realistic components under compressive loading. Firstly, delamination growth in a stiffened panel containing an embedded defect is modelled under post-buckling conditions. This component is representative of CFRP aerospace elements found in wing, fuselage and tail surfaces. Secondly, skin/core debonding from an embedded defect in a sandwich panel is modelled. This is representative of components used in GFRP marine hulls and decking. The local buckling of the delaminated layers, global buckling of the component, initiation and subsequent damage growth are modelled and successfully validated against experimental results.

Introduction

Laminated materials are used in a wide range of applications, but their uptake for primary (safety-critical) components has been limited [1]. This is mainly due to their sensitivity to interlaminar defects, such as delamination in monolithic materials and debonding in sandwich components. This problem is compounded by a shortage of reliable and robust models for predicting the performance of damaged laminated materials. Consequently, current designs are excessively conservative and incur high ownership costs due to the need for frequent inspection and repair. Modelling of delamination and debonding is computationally demanding, with issues such as large deformations, local buckling of the delaminated layers, global buckling of the entire structure and contact across the crack faces needing to be addressed. Such problems are not conducive to analytical simplifications, and a numerical approach (finite element) is the only means by which to capture this behaviour. In general [2], under compressive loading, the out-of-plane deflection of the delaminated layers leads to a combination of peel (mode I), shear (mode II) and tearing (mode III) forces at the defect boundary. If these forces exceed the material fracture toughness, delamination will initiate and grow.

The modelling of global buckling of the structure, local buckling of delaminations and the subsequent contact between delaminated plies and sub-laminates is fairly well understood. These deformations are then input into a failure criterion [2] to predict whether, at a particular load-level, initiation of growth has occurred. A common approach is then to model the actual delamination growth process using node release; the individual nodes at the defect boundary are broken to simulate crack extension. Although this mimics the physical growth process fairly well, it is fraught with problems. Releasing nodes means the stiffness matrix for the mesh needs to be regenerated and the model rerun, which is immensely time consuming [3]. Also, the release of single nodes can lead to discontinuities in the originally smooth delamination front, introducing artificial spikes in the stress distribution around the boundary. Node release is a cumbersome method of modelling delamination and consequently there has been only limited success in using it to model defect growth in laminated components. A variation of this method is to connect the delamination faces with interface elements [4]. The properties of these can be defined to mimic the material behaviour as it fractures. In addition, the area under the load/displacement response of the interface element can be set to be equivalent to the energy for fracture (G_C). However interface elements can give mesh-dependent results [3] and in brittle materials a very fine mesh is required. An approach that

avoids many of these problems is adaptive remeshing [4,9,10] in which the dense mesh required to capture the growth processes moves with the crack front. This ensures the zone at the crack tip is accurately modelled whilst areas away from the crack are modelled efficiently with a course mesh. However, the method can still be time consuming, since the stiffness matrix needs to be reformulated with every growth step.

Finally, a most promising method (and perhaps the most elegant) is the moving mesh approach [11,12,13]. Rather than releasing nodes to mimic growth of the delamination front, the mesh geometry is modified (Figure 1). This means the stiffness matrix does not need to be redefined, so the growth can be modelled efficiently and quickly. This method also avoids discontinuities in the crack front, since the algorithm used to change the mesh geometry ensures the front is smooth. However, the main drawback of this approach is that, since the mesh geometry changes, it is difficult to model features such as changes in thickness, or changes in crack plane.

The objective of the work reported here was to develop and validate the moving mesh approach for modelling delamination. This approach is demonstrated against two experimental benchmarks [3] representative of realistic components under compressive loading. Firstly, delamination growth in a stiffened panel containing an embedded defect is modelled (Figure 2). Secondly, skin/core debonding from an embedded defect in a sandwich panel is modelled (Figure 3). The local buckling of the delaminated layers, global buckling of the components, initiation and subsequent damage growth were modelled and successfully validated against experimental results.

Details of the Numerical Modelling

Simulation of delamination buckling and growth was carried out using the finite element based programme package DEBUGS (DElamination BUckling Growth and Simulation). DEBUGS is based on a shell element formulation and uses the commercial FE code ADINA. The model accounted for the effects of global bending of the structure and contact between the delaminated plies. The development of DEBUGS has been described elsewhere [11,12,13] and only a synopsis of the main features is given here. Two kinematically non-linear shear deformable plates model the delaminated skin. In the undelaminated domain, the upper and lower plates are constrained by a displacement continuity along the 'interface'. In the delaminated domain, delaminated members are free to deflect from each other but constrained not to penetrate by means of contact springs. Stiffeners are also modelled by shell elements connected by constraint equations similar to those used for the undelaminated skin. Delamination growth is assumed to take place when the energy release rate reaches a critical value. Mixed mode interface crack growth is expressed as $G = G(\psi)$, where ψ is the phase angle defined by $\psi = \tan^{-1}(K_{II}/K_I)$. The energy release rate at local crack growth, G, can be computed from the discontinuity in field variables across the crack front:

$$G = \left(P_{nn}^{(1)} - P_{nn}^{(2)}\right) + \left(P_{nn}^{(3)} - P_{nn}^{(4)}\right) \text{ where } P_{nn}^{(h)} = W^{(h)} - N_{n\gamma}^{(h)}\overline{u}_{n,\gamma}^{(h)} - Q_n^{(h)}\overline{u}_{3,n}^{(h)} - M_{n\gamma}^{(h)}\theta_{n,\gamma}^{(h)}$$

The superscript denotes the location of the tensor, P_{nn} and where W is the strain energy function, N, M and Q denote membrane forces, transverse shear forces and moments respectively; $\overline{u}_i$ is the midplane displacement and θ transverse rotation; n denotes the normal direction to the crack front; double Greek indices denote summation of normal and tangential components.

A complete analysis of delamination buckling and growth includes the following steps:

- The global (plate) buckling load is first determined for the structure.
- The delamination buckling load is subsequently determined with due account for contact.
- A kinematically non-linear postbuckling analysis using a full Newton method and a contact analysis is performed at each load. Once the contact analysis has converged, the energy release rate is computed along with fracture mode separation. Load increments are taken automatically such that they are small near the delamination and global buckling loads (where the tangential stiffness may be very low). The load increments are also adjusted such that the crack growth criterion is attained but not significantly exceeded.

- The delamination front will propagate when the crack growth criterion has been met at some node. The front is then advanced by moving the nodes which have reached the crack growth criterion a small distance in the local normal direction to the front, followed by a second step where the entire mesh is slightly moved. The postbuckling analysis is then restarted at the previous propagation load, but with the new updated mesh.

By this method, the delamination growth is modelled by performing a large number (typically in the order of a few hundred) of incremental crack propagations. The mesh is moved by solving a two-dimensional finite element problem using the same mesh as in the shell analysis. Nodes along the delamination front, which have attained the crack growth criterion, have prescribed displacements equal to the crack increments. Nodes along the front which have not attained the crack growth criterion have zero prescribed displacements. The new nodal co-ordinates for the shell problem are taken as the nodal co-ordinates after deformation of this two-dimensional problem.

Numerical Models (Stiffened Panel)

The model for the stringer-stiffened panel (Figure 4a) was also based on previous experimental work [3]. The panel was made from Hexcel T800/924, with a skin stacking sequence of $[(+45°/-45°/0°/90°)_3]_S$ and a ply thickness of 0.125mm. During manufacture, circular PTFE inserts (10μm thick and 50mm diameter) were placed at the desired interface, in the centre of a bay. Two numerical simulations were carried out; one panel with a defect (Figure 4b) three plies deep (0°/90° interface), and one with a defect five plies deep (45°/-45° interface). Previous modelling studies [2,11] had shown that, for all these cases, the delamination was driven by mode *I* dominated loading. Consequently a value of $G_C = 248J/m^2$ was chosen [2]. The panels were under uniaxial load in the direction of the 0° plies (the global *x*-direction). They were loaded along one edge, whilst the opposite edge was fixed to movement in the *x*-direction. The following measured properties of T800/924 [2] were used: E_{11}=155GPa, E_{22}=8.57GPa, ν_{12}=0.33 and G_{12}=7.4GPa. The remaining mechanical properties were assumed: $E_{33}=E_{22}$=8.57GPa, $\nu_{13}=\nu_{12}$=0.33, ν_{23}=0.52, $G_{13}=G_{23}$=7.4GPa. The simulations were carried out on a Silicon Graphics Octane with 256 MB of memory, running 64-bit IRIX version 6.5.

Figure 4c shows the global panel buckling, which was found to agree with that observed in previous studies [3]. The results are tabulated in Table 1 whilst Figure 5 shows a number of results: a) the out-of-plane displacement of the defect centre; b) contours of growth. Finally, Figure 6 shows the initiation and rate of growth for both the experimental and predicted behaviours. The global and local buckling predictions were accurate, exhibiting rotation of the delamination as seen in the experimental studies. The position of the peak G_C for the defect at the 0°/90° ply interface was close to the lateral boundary (90° and 270° positions), as identified before, whilst that for the +45°/-45° ply interface was wider and close to the 105° position. The predicted initiation strains were higher than those observed in the experiments; Figure 6. However, the rate of growth after initiation was similar to that observed experimentally. Although the delamination at the 0°/90° ply interface had initiated at a lower strain, the growth rate was less than that for the delamination at the +45°/-45° ply interface. Most of the growth was close to the lateral boundary of the defect.

Numerical Models (Sandwich Panel)

A quarter-symmetry model for the sandwich panel is shown in Figure 7a; this was based on recent experimental work [4]. The panel consisted of a 2.63mm outer skin of 300gsm CSM, 4xDEVOLD DBL800 (GF tri-axial), 100gsm CSM; a 40mm thick end-grain balsa core (D150); and a 2.56mm inner skin; 100gsm CSM, 4 x DEVOLD DBL800, 100gsm CSM. Figure 7b shows an isometric view of a portion of the panel, giving a visual indication of the representative thicknesses. A circular PTFE insert (10μm thick) was in the centre of the panel, between the outer skin and the core. The whole panel was infused with Reichhold Norpol Dion 9500-510; a rubber modified vinylester. Panels were manufactured with different two defect sizes: 300mm and 600mm diameter. In the absence of G_C values the mode I fracture toughness between glass polyester skin and balsa core was obtained elsewhere [5]; $G_{IC}=1150J/m^2$. The following measured properties of a single ply of DEVOLD material [6] were used: E_{11}=42.6GPa, E_{22}=9.2GPa, ν_{12}=0.26, G_{12}=1.33GPa and

G_{13}=G_{23}=3.0GPa. The remaining mechanical properties were assumed: E_{33}=E_{22}=9.2GPa, ν_{13}=0.26, ν_{23}=0.5. The thickness-layer orientation for DBL800 [6] is: 0.293mm 0°/0.144mm 45°/0.007mm 90°/0.144mm –45°. The measured properties for CSM [6] were: E=13.8GPa and ν=0.3. The balsa core (D150) properties [7] were given as: E_{11}=E_{22}=0.293GPa, E_{33}=6.183GPa, ν_{12}=0.45, ν_{13}=ν_{23}=0.0171, G_{12}=1.066GPa and G_{13}=G_{23}=0.315GPa. The computations were carried out on the Silicon Graphics workstation described above.

The results of the simulation and the experimental observations [4] are tabulated in Table 2. Figure 8 shows a number of results: a) the out-of-plane displacement of the defect centre; b) contours of growth. Figure 9 shows the initiation and rate of growth for both the experimental and predicted behaviours. For both cases, the position of the peak G_C on the boundary before growth was at the 90° and 270° positions. This was primarily the result of a local buckle 'blister' forming perpendicular to the directions of loading; this was seen in the experiments [4]. The predicted initiation strains for the panel with the 600mm diameter defect was accurate to within 14% and the panel with the 300mm diameter defect showed a 17% error. Rate of growth predicted was similar to the growth rate seen in the experiments [4].

Discussion

In general, the modelling results for the stiffened panels were satisfactory, although they fall short of a reliable predictive tool for delamination growth. The panel buckling, local buckling shape of the delaminated plies, and the contact between these plies and the sublaminate were successfully modelled. However, the models did not predict the initiation strain for delamination growth very well. This was attributed to a number of factors, most important of which was the presence of ply cracks at the delamination boundary; these have been identified experimentally. These cracks promoted initiation of delamination growth, which led to a reduction of the initiation strain. This factor was particularly important for the defects at the 0°/90° ply interface [2] which accounted for the larger discrepancy for the laminates with the defect at this interface. In addition, in the experimental studies, the growth was observed to have been at an angle to the defect boundary, and not normal as assumed by the model. Consequently, the models were non-conservative for predicting initiation of delamination growth.

As in the skin stringer panels, the global response of the sandwich panels, the local buckling shape of the delaminated skin, and the contact between the skin and the core were successfully modelled. Again, the models did not predict the initiation of strain for growth of the delamination very well. This may be attributed to a number of factors: the G_C value used was assumed; the actual material properties of the experimental panel may differ from those in the literature; the panel dimensions in the computation were nominal and not actual.

The final aspect of the modelling was the growth of the delamination, which was one of the primary reasons for using a moving mesh approach. The growth rates and shapes of the delaminations were similar to those observed, which is very encouraging. The models also captured differences in the behaviour due to the structural conditions. For example, the buckling of the sublaminate was simulated (Figure 5a and Figure 8a), which would contribute to the mixed-mode conditions at the defect boundary. For the skin-stringer model, the effect of global structural buckling was captured. This would have superimposed upon the delaminating conditions, leading to the greater peak in G_C on one side of the defect (Figure 5b).

The key drawback of the moving mesh approach is the problem of freezing a site such that it does not move as the mesh geometry changes. This introduces difficulties in a number of areas. Firstly, the sites of ply cracking and element degradation will need to be fixed, which may be problematic if close to the delamination front. Also, changes in geometry such as thickness or delamination interface can cause difficulties, since these will need to be frozen as the mesh changes geometry.

Improved Modelling of the Physics of Delamination Growth

The current philosophy to modelling delaminations is to assume the damage growth remains within

the defect plane. However experimental and fractographic studies [2] have indicated that this approach is flawed, and the actual growth processes are very different. Almost without exception, the direction of delamination growth will be parallel to the one of the plies of the interface rather than normal to the defect boundary [2]. The mechanism is given in detail elsewhere [2,11] but to summarise, the local crack tip conditions at the defect boundary acts to drive the delamination through the thickness of the laminate. Consequently the delamination migrates through the layers until it reaches an interface in which the direction of the driving force and fibre orientation are approximately coincident (<10° [14]). Whether the delamination migrates upward through the plies, or down into the laminate is dependent on the bending direction of these plies [15]. If the delamination does not migrate to a preferential interface, the load will increase until the component of the driving force parallel to the controlling fibres exceeds the toughness in that direction. The delamination will then grow within this interface parallel to these fibres (at an angle to the driving force), albeit at a reduced rate. A consequence of this process is that the material toughness does not need to be characterised over a spectrum of ply orientations. The toughness of the material can just be characterised at two or three 0°/ϕ° ply interfaces since, locally to the crack tip, for delamination growth the controlling ply is always a 0°. For example, for the [±45/0°/90°] family of laminates, only the toughness of the 0°/45° and 0°/90° ply interfaces needs to be characterised. A detailed characterisation of this migration process is currently underway [16].

As well as addressing ply cracking, realistic modelling of the delamination growth also needs to be addressed. Rather than assuming growth is normal to the defect boundary, models need to incorporate the controlling effect of the fibre orientation. The simplest approach to account for this effect would be to multiply the critical strain energy release rate (G_C) by a function $T(\alpha)$ to give an apparent toughness G'_C, where α is the angle of the normal to the defect boundary (with respect to the 0° ply). When α is equal to the ply direction, T is unity, but as α moves away from this, T becomes large and the apparent toughness will be very high. However, this model would still predict growth as normal to the boundary, which is not physically correct. Also, the shape of the function $T(\alpha)$ would require extensive fracture toughness testing which would be expensive.

A more physically realistic approach would be to redefine the mode *I, II* and *III* components with respect to the controlling ply direction rather than the boundary of the defect. This requires modification of the definition of the mode *I, II* and *III* used in the virtual crack closure (VCC) calculation (Figure 10); α is the angle of the normal to the boundary and ϕ is the direction of the controlling ply; the difference between these two directions is defined as an angle β. In the conventional VCC calculation the nodes *(a)* and *(b)* were used to determine the pure mode components. However, in the refined model, the pure mode components are aligned with the controlling fibre direction (shown in red). Therefore, a point *(c)* is defined (Figure 10) which is the same distance, Δ, as *(b)* from the boundary, but is aligned with the controlling ply. The position of *(c)* is (x_c,y_c) and is given by;

$$x_c = x_a - \xi\ \Delta\ \cos\phi \ \text{ and } \ y_c = y_a - \xi\ \Delta\ \sin\phi \qquad \text{where } \xi = \frac{\cos(\phi-\alpha)}{\left|\cos(\phi-\alpha)\right|}$$

The mode *II* is defined as parallel to the controlling ply, and mode *III* is defined as perpendicular to this ply. The consequence of this modified calculation of the pure mode components is that the delamination may still initiate from the site of the highest driving force, but will extend along the fibre directions, as observed in the experiments.

Conclusions

Based on the development of the moving mesh approach for modelling delamination and validation of these models against experimental benchmarks, the following conclusions were drawn.

1. The moving mesh model used 2D composite shell elements in 3D space, joined by multipoint constraint (MPC) equations and rigid links (limited to two layers).
2. The moving mesh approach was successfully validated against experimental data from tests on flat sandwich panels (skin/core defects) and stiffened panels (embedded skin defect).

3. The models successfully predicted the panel buckling, the local buckling shape of the delaminated plies, and the contact between these plies and the sublaminate.
4. Difficulties were encountered with predicting initiation of delamination growth which was attributed to the physics of the crack initiation process not being captured. However, the models successfully predicted the growth rate and direction for both experimental benchmarks.
5. Although the moving mesh approach offers an elegant and efficient solution to predicting delamination growth, it is limited to modelling single plane growth and will encounter problems when modelling damage approaching changes in laminate thickness.
6. To improve the accuracy of future delamination models, mechanisms such as migration of the delamination through the laminate and the influence of ply orientation need to be accounted for. A formulation has been suggested to address the latter, but this needs to be further developed to allow implementation in predictive models.

Acknowledgements
The authors would like to acknowledge the support of the DTI Aeronautics Research Programme (CARAD) and the MoD Corporate Research Programme.
© Copyright QinetiQ Ltd 2004

References
1. Heath, B., '*ADSTREFF (Advanced Structural Efficiency) – State of the Art Review*', Targeted Research Action, Brite/Eurem III, Airbus UK, BETC 1021BETC 1039, 2000.
2. Greenhalgh, E., "*Characterisation of mixed-mode delamination growth in carbon-fibre composites*", PhD Thesis, Imperial College, London, 1998.
3. Wiggenraad, J., '*GARTEUR AG22; Design Methodology for Damage Tolerant Composite Wing Panels*', Final Technical Report, GARTEUR TP-122-6, NLR-TR-2001-413, 2001.
4. Lord, S, 'THALES Joint Programme – Supplement JP3.23 Inspection and Repair of Sandwich Structures in Naval Ships (saNDI) 2000-2004', QinetiQ report to be published, 2004
5. de Vries, L.B., *WP2.1 Report on Material Selection and Material Characterisation Programme Specification.* EUCLID TNO Report TNO-2.1-J1-IP2.0, 2001.
6. Cusano, G., *Finite element modelling and simulations of external blast test on 3D composite structure.* CETENA SpA Report No. CET-2.2-J5-IP1.0, 2002.
7. van Aanhold, J.E., TNO Centre for Maritime Engineering. Private communication, 2002.
8. Willows, M., '*ADCOMP (Adaptive Composite Delamination Modelling) - Final Technical Report*' BE-3580, Brite/Eurem III, 18th Sept 2000.
9. Roudolff, F. & Gadke, M., '*Damage Tolerance of LTA Composite Structures*', 1st ONERA/DLR Aerospace Symposium, Paris, France, June 21-24, 1999.
10. Kruger, R., Minguet, P. & O'Brien, T, '*Implementation Of Interlaminar Fracture Mechanics In Design: An Overview*', 14th International Conference on Composite Materials (ICCM-14), San Diego, July 14-18, 2003.
11. Greenhalgh, E., Singh, S. & Nilsson, K-F., '*Mechanisms and Modelling of Delamination Growth and Failure of Carbon-Fibre Reinforced Skin-Stringer Panels*', ASTM STP 1383 & ASTM D-30, 'Composite Structures: Theory & Practice', Seattle, Washington, USA, 2000.
12. Nilsson, K-F., Asp, L. & Alpman, J., "*Delamination buckling and growth at global buckling*", First International Conference on Damage and Failure of Interfaces, Ed. H.-P. Rossmanith, Vienna, pp193-202, 1997.
13. Alpman, J. & Nilsson, K-F., '*Manual and Description of DEBUGS 1.0; Delamination Buckling and Growth Simulation*', FFAP-H-1402, FFA, The Aeronautical Research Institute of Sweden, 1999.
14. Nilsson, S., '*Compression Tests of Composite Panels with Embedded Defects*', FFA-TN2000-74, The Aeronautical Research Institute of Sweden, 2000.
15. Nilsson, K-F., Asp, L. & Sjogren, A., '*On transition of delamination growth behaviour for compression loaded composite panels*', FFA TN-2000-19, The Aeronautical Research Institute of Sweden, 2000.
16. Datta, S., Robinson, P. & Hitchings, D., '*Development Of Translaminar Migration And Fatigue Facilities In A Fe-Based Delamination Growth Model*', QinetiQ Contract CU4/26430, 2004.

Simulation	Initial delamination details			Delamination initiation strain (με)	
	Diameter	Interface	Depth	Observed	Predicted
#1	50mm	0°/90°	3 plies	-3985	-2500 (35mm defect)
#2	50mm	+45°/-45°	5 plies	-3292	-2850

Table 1 Details of initial defects and delamination initiation strains in stringer stiffened panels

		Experiment	*Predicted*		
Simulation	**Initial defect diameter**	**Initiation strain (με)**	**Initiation strain (με)**	**Stable growth**	**Failure strain (με)**
#3	300mm	-4336	-3615	Up to 15mm	< -4275
#4	600mm	-2691	-3065	Up to 14mm	< -3500

Table 2 Details of initial defects and delamination initiation strains in sandwich panels

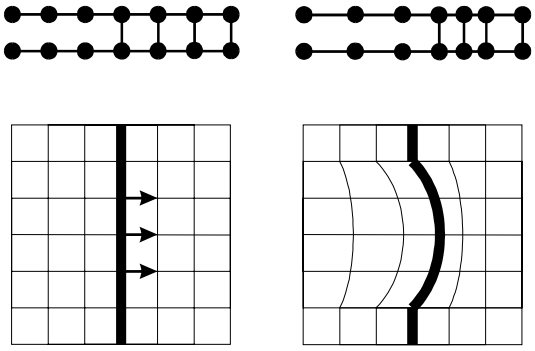

(a) (b)

Figure 1 Methods of modelling propagation of delamination; (a) before growth and (b) after growth

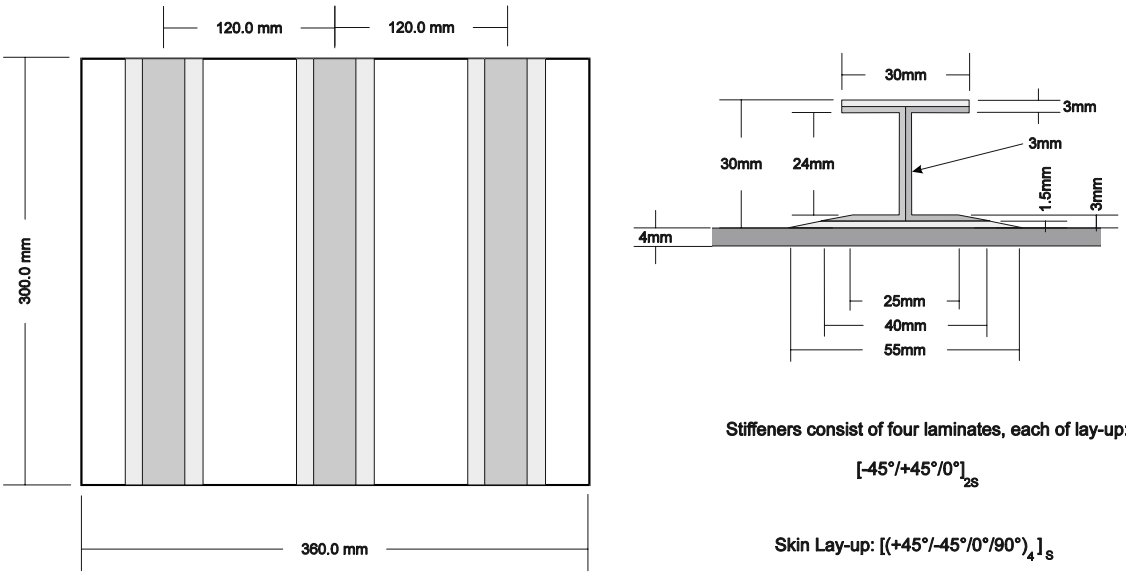

Figure 2 Geometry of the skin-stringer panel

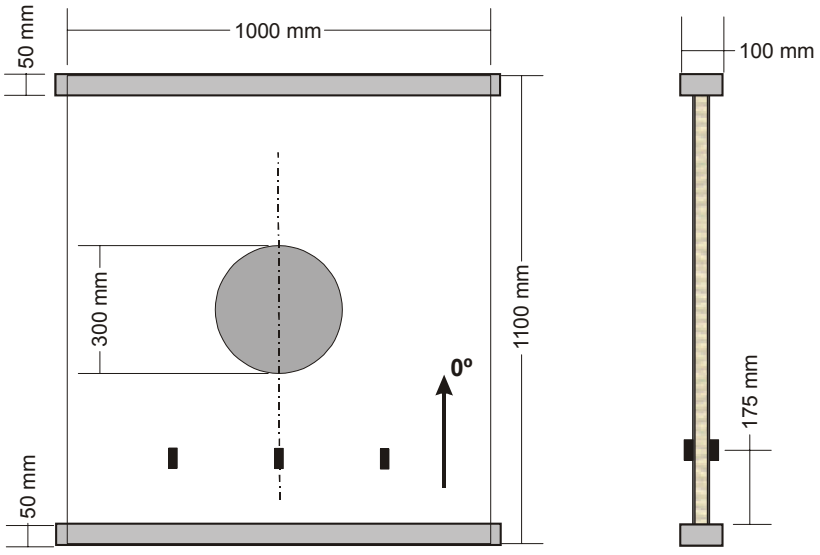

Figure 3 Geometry of the sandwich panel

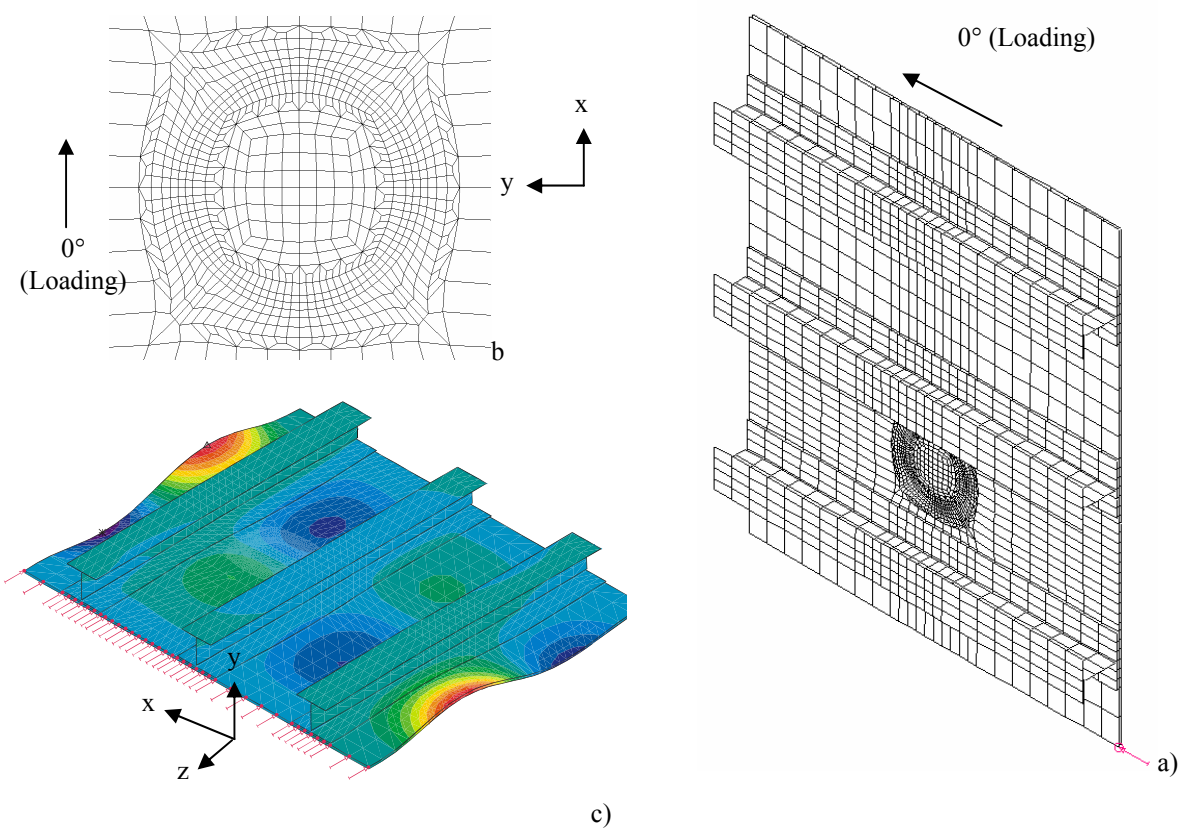

Figure 4 Finite element mesh of the panel with a 50mm diameter embedded defect

defect at 3/4 ply interface (0°/90°)

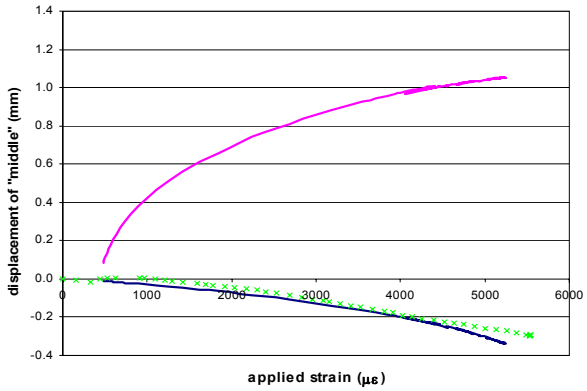

defect at 5/6 ply interface (+45°/-45°)

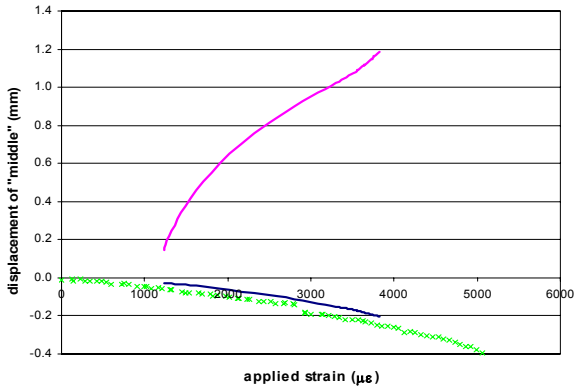

a) Out-of plane displacement for defect centre against applied strain for the delaminated plies (purple) & the sublaminate (blue-model; green-experiment [3]))

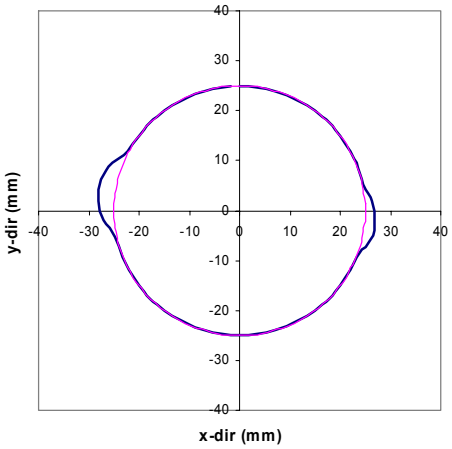

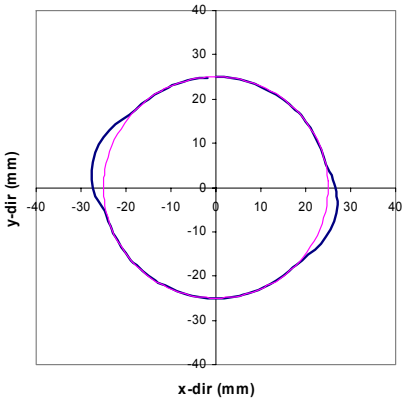

b) The delamination for the original defect (purple) and final growth (blue)

Figure 5 Results for stringer stiffened panels

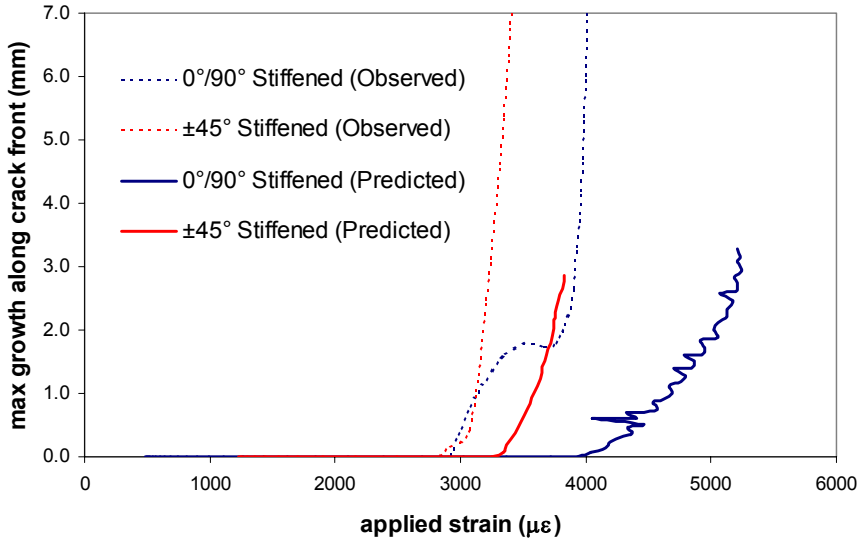

Figure 6 Observed and predicted growth against applied strain for the stiffened panels

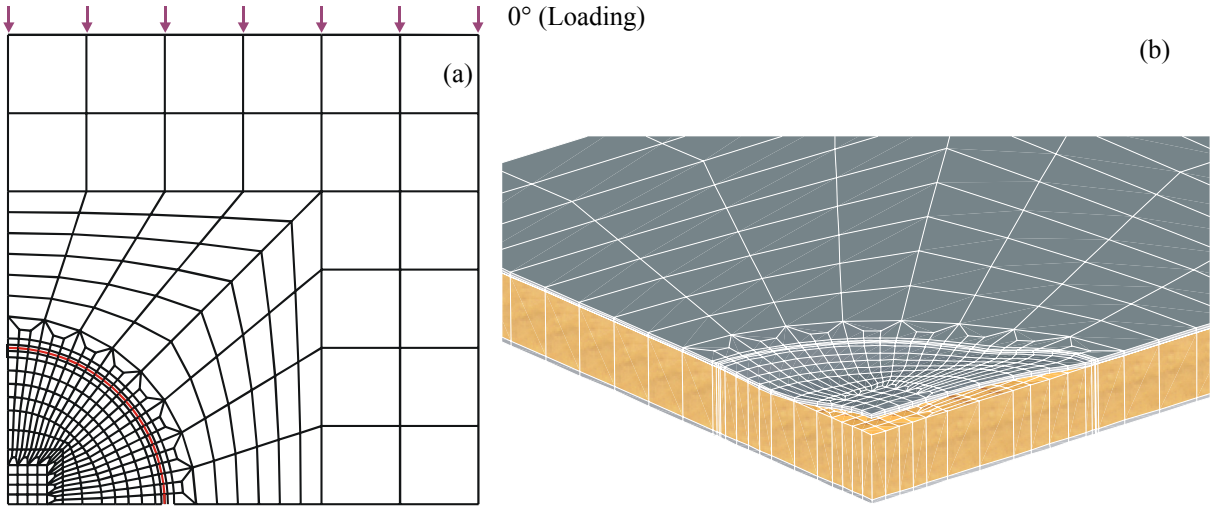

Figure 7 ¼-sym finite element mesh of sandwich panel with a 300mm diameter embedded defect

300mm diameter defect

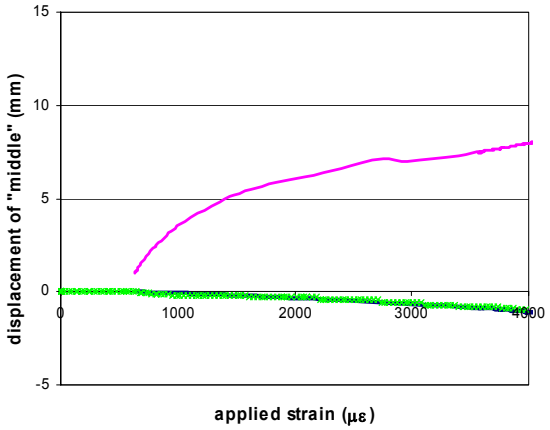

600mm diameter defect

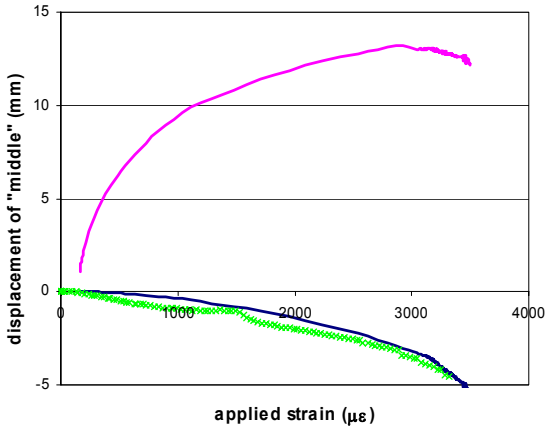

a) Out-of plane displacement for defect centre against applied strain for the debonded outer skin (purple) & the core/inner skin (blue-model; green-experiment [4])

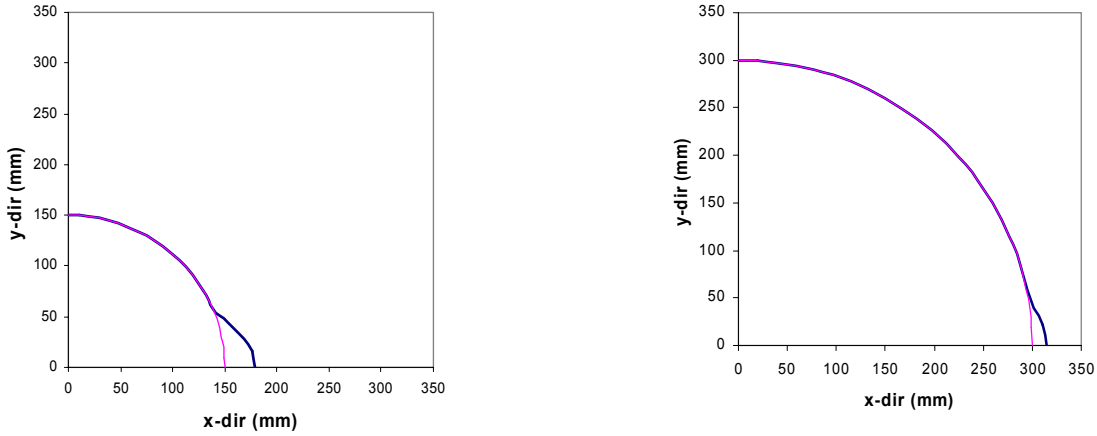

b) The delamination for the original defect (purple) and final growth (blue)

Figure 8 Results for sandwich panels

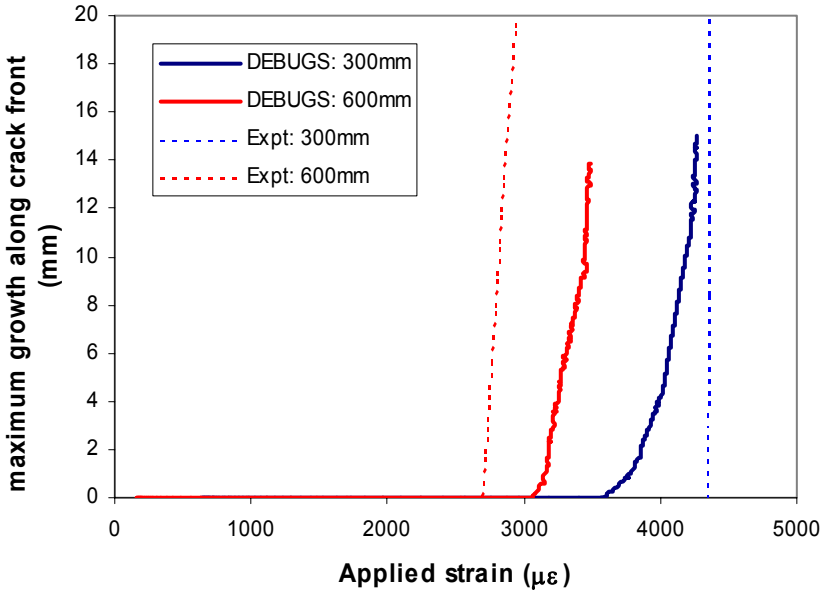

Figure 9 Observed and predicted growth against applied strain for sandwich panels

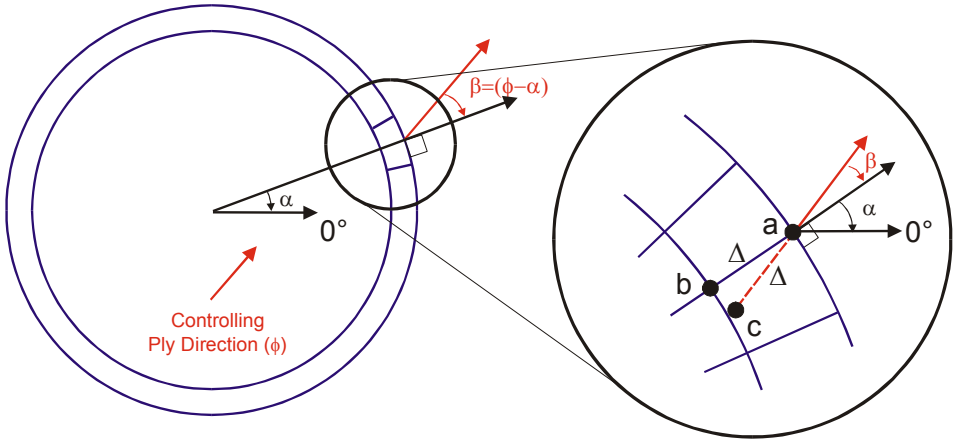

Figure 10 Redefined nodal positions for determining G_I, G_{II} and G_{III} for the delamination model